Bacterial cellulose coated ST-cut quartz surface acoustic wave humidity sensor with high sensitivity, fast response and recovery

J L Wang[a], Y J Guo[a,*], D J Li[a], G D Long[a], Q B Tang[a], X T Zu[b], J Y Ma[c], B Du[c], Y L Tang[d,*], H. Torun[e], Y Q Fu[e,*]

[a] School of Physics, University of Electronic Science and Technology of China, Chengdu, 610054, P. R. China

[b] Institute of Fundamental and Frontier Sciences, University of Electronic Science and Technology of China, Chengdu, 610054, P. R. China

[c] Sichuan Institute of Piezoelectric and Acousto-Optic Technology, Chongqing, 400060, P. R. China

[d] School of Physical Science and Technology, Southwest Jiaotong University, Chengdu, 610031, P. R. China

[e] Faculty of Engineering & Environment, University of Northumbria, Newcastle upon Tyne, NE1 8ST, UK

Abstract:

A Love mode surface acoustic wave (SAW) humidity sensor based on bacterial cellulose (BC) coated ST-cut quartz was developed in this study. The BC film is composed of ultrafine interwoven fibers to form a highly porous network, and its surface contains a large amount of hydroxyl groups, which significantly improve the adsorption capability of SAW sensing layer for water molecules. This results in significant mass loading effects and enhanced responsivity of the SAW sensor. The

resonant frequency of the sensor changes linearly with RH at lower relative humidity (RH) values (e.g., RH<30%), but when RH>80%, an exponential increase in frequency shift as a function of RH is obtained due to the enhanced mass loading effect. A frequency shift of 89.8 kHz was measured using a sensor with a BC film with a thickness of 148 nm thick when the RH was increased from 30% to 93%. The frequency of the sensor can be fully shifted back to the original reading when the RH was returned back to 30%, with the response and recovery times of 12 s and 5 s, respectively. The SAW sensor also exhibits good short-term repeatability and long-term stability for humidity sensing.

Keywords: Bacterial cellulose (BC); SAW sensor; Humidity; Fast response and recovery.

*Corresponding authors and E-mail addresses:

Prof. Yuanjun Guo (guoyuanjun@uestc.edu.cn); associate Prof. Yongliang Tang (tyl@swjtu.edu.cn); Prof. Richard Yongqing Fu (richard.fu@northumbria.ac.uk).

1. Introduction

Precise and quantitative monitoring of humidity is critical for various industries including manufacturing, agricultural production, environmental testing and aerospace technology, which demand humidity sensors with high precision, fast response, and good stability [1-4]. In recent years, humidity sensors based on various transduction principles have been developed, mainly including resistive, capacitive, ultrasonic, and surface acoustic wave (SAW) sensors [5-8]. The SAW humidity sensor has advantages of high precision, small size and good stability. Meanwhile, it is suitable for

wireless operation, which is especially important for the detection of humidity in harsh environments [9].

SAW devices fabricated on different piezoelectric substrates have been reported for humidity sensing. For example, Le et al. [10] demonstrated a SAW humidity sensor on an AlN/Si substrate and Liu et al. [11] reported a SAW humidity sensor on a $LiNbO_3$ substrate. However, these sensors are highly temperature dependent and have a low thermal stability. Temperature coefficient of frequency (TCF) determines the frequency stability with temperature, and lower TCF values are required for improved performance of the SAW sensors. Otherwise, variations in temperature may result in significant frequency shifts, which will interfere with the those due to the changes in humidity. Among different candidates for the SAW substrates, the ST-cut quartz is ideal for humidity sensing owing to its nearly zero TCF. For example, Tang et al. [12] reported a SAW humidity sensor on the ST-cut quartz substrate, exhibiting both good thermal stability and sensitivity.

Bacterial cellulose (BC) is one of the emerging functional nanomaterials with important applications in biotechnology and materials science [13-16]. It is a filamentous and fibrous by-product secreted by microorganisms such as acetobacters and agrobacteria [17,18]. Synthesis rate of BC is generally much higher than that of photo-synthesis of cellulose in plants, thus BC has advantages of being low cost and environmentally friendly [19]. By adjusting the conditions of the growth culture or metabolic pathways of microorganisms, it is possible to synthesize BCs with specific morphologies, thereby modifying functional properties of BC-based nanomaterials for the targeted applications [20]. BC has excellent water retention capabilities as its surface contains a large number of hydrophilic groups, which can absorb water molecules. In addition, BC films have excellent thermal stability and relatively higher Young's moduli compared to those of polymers

[21,22]. For example, Hu et al. [23] developed a BC humidity sensor based on a quartz crystal microbalance.

A major research for SAW humidity sensor is the development of new sensing layer materials with improved sensitivity and selectivity [24,25]. Various materials, such as polymers, metals, and metal oxides have been reported as coating layers on SAW sensors for the detection of humidity and gasses [9,26]. Yet, a BC sensing layer has never been reported in SAW sensor as far as we know. In this paper, a SAW humidity sensor based on BC coated ST-cut quartz substrate is developed, which shows a significant mass loading effect and significantly enhanced performance.

2. Experimental details

21 SAW resonator and BC sensing layer

SAW resonator based humidity sensors, as shown in Fig. 1(a), were fabricated on ST-cut (42°75') quartz substrate (12 mm × 3 mm × 0.5 mm) and consists of periodic aluminum interdigital transducers (IDTs, 30 pairs), reflective gratings (100 pairs), and a sensing layer coated between the IDTs. The IDTs have a finger width of 4 μm and an aperture of 3 mm. The center frequency of the designed SAW resonator is 200 MHz. The transmission spectrum (S_{21}) of the SAW resonator, measured between the ports of IDTs, is shown in Fig. 1(b), revealing a low insertion loss of -8.486 dB.

The sensing layer of the SAW device is prepared from the cultured BC using a sol-gel and spin coating method. Acetobacter xylinum was placed in a medium containing 2% glucose and 2% corn syrup. The oxygen-enriched air was introduced into the solution. The pH value of the medium was adjusted to 5.5, and the temperature was controlled at 28°C. The BC crude product was extracted

after a static culture duration of 8 days. After washed with distilled water, 0.1 mol/L NaOH was added inside the above solution and the solution was kept at 80^{o}C for 30 minutes to obtain a purified content of 0.65 wt.% BC. The BC with a volume of 46.2 ml and 0.65 wt.% was diluted in 150 ml of deionized water at room temperature of 25^{o}C. The mixture was mechanically stirred for 2 hrs and aged for 24 hrs to prepare a BC hydrogel with a BC content of 2‰. The prepared BC hydrogel was spin-coated onto the SAW device at 6000 rpm for 30 seconds, and dried at 60^{o}C for 8 minutes to obtain a uniform BC film. BC films with different thicknesses were prepared by multiple spin coating processes (e.g., one layer, three layers, five layers, and seven layers, with the corresponding device names of Layer-1, Layer-3, Layer-5, and Layer-7). Finally, the SAW resonator coated with a BC film was connected to an oscillator circuit to constitute a SAW sensor.

22 Characterization and humidity sensing

Surface morphology of the BC was characterized using a field emission scanning electron microscope (FE-SEM, FEI Inspect F50). Surface functional groups of the BC were characterized using Fourier transform infrared spectroscopy (FTIR, Nicolet IS 10, ThermoFisher Scientific). The specific surface area and porosity of the BC was measured using a Brunauer-Emmett-Teller surface and a nitrogen adsorption analyzer (Micromeritics ASAP 2020). The electrical conductivity of the BC-based sensing membrane was measured using a four-point probe and a digital source meter (Keithley 2400, Tektronix). A vector network analyzer (Hewlett-Packard 8714C) was used to obtain the electrical parameters of the SAW device. Temperature and humidity of the testing chamber were measured using a hygrothermometer (LH-331BL).

Figure 2 shows experimental setup for the humidity sensing. Temperature and relative humidity

(RH) of the experimental environment were controlled to be 25ºC and 30%, respectively. Five different saturated salt solutions were filled into five testing chambers with a fixed volume of 20 L to control the RH according to the international standard for RH control [27]. Experiments were performed by rapidly inserting the BC SAW humidity sensor into the closed chambers with different RH values, and by quickly taking the sensor out from the chamber. A frequency counter (Agilent 53210A) was used to measure the SAW frequency. For each RH value, the sensor was repeatedly tested for three times, and the averaged reading was obtained.

3. Results and discussions

3.1 Characterization of BC films

Fig. 3 shows the SEM images of the deposited BC films, which reveal ultra-fine reticular fiber structures comprised of interwoven ribbons with diameters of 40-60 nm. The measured thicknesses of the Layer-1, Layer-3, Layer-5, and Layer-7 BC films are about 61, 84, 112, 148 nm, respectively. Large numbers of nanopores are present within the cellulose ribbons of the film.

Fig. 4(a) shows the analysis results of functional groups of the BC materials using FTIR. The peaks at 3332 cm^{-1} and 1314 cm^{-1} are related to the tensile vibration modes of O-H and C-OH bonds, respectively. The peaks at 2896, 1590, and 1029 cm^{-1} are due to C-H antisymmetric stretching vibration, H-C-H deformation vibration and C-N stretching vibration, respectively. Among these, only those of O-H and C-OH bonds strongly influence the humidity sensing capability as reported in Ref. [28]. Analysis results clearly show that the surface of the BC contains a large amount of hydroxyl groups. The BET analysis results of the BC materials are shown in Fig. 4(b). The specific surface area of BC was measured to be 103 m^2/g with average pore diameter of 35.4 nm and the

meso-porosity of 63.1%.

Based on these analysis, Fig. 5 depicts a conceptual drawing for the response of these BC membranes when exposed to water molecules. Water molecules easily penetrate these three-dimensional network structures of the BC film with a large number of pores. A large number of hydroxyl groups on the surface of the BC strongly enhance the adsorption water molecules, and then form hydrogen bonds, thus providing a good water retention capacity.

3.2 Sensing measurement results and mechanisms

The measured shift in resonant frequency of the SAW devices is mainly due to the changes in wave propagation velocity, which is strongly influenced by the environmental factors such as humidity and temperature. The working mechanisms of a SAW device generally include mass loading effect, electrical loading effect and viscoelastic loading effect [29-31]. During the experiments, we precisely controlled the temperature and atmospheric pressure, and only changed the RH value. The adsorption of water molecules in the BC layer does not make it significantly stiffer or softer, therefore, the viscoelastic loading is not significant.

Electrical loading effect of a film refers to the phenomenon that the change in the conductivity of the film causes a change in the SAW velocity and thus the resonant frequency. The relationship between the change in the resonant frequency (Δf) and the conductivity of the film surface (σ_s) can be described as [32]:

$$\frac{\Delta f}{f_0} = \frac{\Delta v}{v_0} \approx -\frac{k^2}{2}\left(\frac{\sigma^2}{\sigma_s^2 + v_0^2 c_s^2}\right) = -\frac{k^2}{2}\left(\frac{1}{1+\left(\frac{v_0 c_s}{\sigma_s}\right)^2}\right) \quad (1)$$

where f_0=200 MHz is the natural resonant frequency of the SAW device; k^2=0.11% is the electromechanical coupling coefficient of the quartz crystal; v_0=3158 m/s is the undisturbed surface wave velocity of the quartz crystal; c_s=0.5 pF/cm is the sum of dielectric constants of substrate and environment.

Fig. 6(a) shows the acousto-electrical parameters ($\xi=\sigma_s/(v_0 \cdot c_s)$ of the SAW sensing layer as a function of the center frequency. The BC film is insulating. The conductivity values of the film measured by the four-probe method in 30% RH and 93% RH are 8.5×10^{-11} and 5.2×10^{-10} Sm^{-1}, respectively. As it is well-known, sensitivity of electrical loading effect of the film depends on the slope of the test point in Fig. 6. Only when the ξ value of the test point is at large slope (high sensitivity) region of 0.1-10, the electrical loading of the film will have a significant effect. Since the conductivity of the BC is extremely low, the frequency shift caused by the acoustoelectric effect was calculated to be only ~1.16 Hz when the RH value was changed from 30% to 93%. The resistance value of R_0 at 30% RH shown in Fig. 6(b) is comparable to that at 93% RH, which further verifies that there is no significant change in the resistance value of the sensing film. Therefore, the significant change in the resonant frequency of the SAW device as a response to RH change is not caused by the electrical loading effect.

Therefore, the mass loading effect due to the adsorption of water molecules into the BC film might be the main reason for the significant changes in the resonant frequencies of the SAW humidity sensor. The relationship between the change in the center frequency (Δf) and the change in the mass of the sensing film (Δm) can be described as follows [33]:

$$\Delta f=(\kappa_1+\kappa_2)f_0^2\Delta m \quad (2)$$

where f_0 is the center frequency of the SAW sensor, which is ~200 MHz in this study, κ_1=-8.7×10^{-8}

m^2skg^{-1} and κ_2=-3.9×10^{-8} m^2skg^{-1} are the matrix constants of the ST-cut quartz. Since both the values of κ_1 and κ_2 are negative, the increased mass loading of the BC film due to the adsorption of water molecules results in a negative frequency shift.

Fig. 7(a) shows the resonant frequency shifts of the SAW devices with different thicknesses of the BC layer when the RH is increased from 30% to 93%. Results show that all the SAW sensors exhibit negative frequency shifts as the humidity is increased. However, the frequency shift without the BC film was measured to be ~2.3 kHz, which is much lower than that of the sensor coated with the BC film. The frequency shift increases significantly with the thickness of the BC film (Fig. 7b). For the SAW resonators coated with 1 layer, 3 layers, 5 layers, and 7 layers of the BC, the insertion loss values were measured to be -16.3 dB, -19.4 dB, -24.2 dB, -28.7 dB, respectively. When the number of layers of BC exceeds 7 layers, the insertion loss of the resonator exceeds -30 dB, and the quality of the vibration signal becomes very poor. Therefore, the SAW sensor coated with 7 layers of the BC was used in the further studies as it has the largest frequency shift.

Fig. 8(a) shows the average values of dynamic responses of 7-layer BC SAW sensors (obtained from three same batch of devices) at different RH levels. When the RH was increased from 30% to 43%, 56%, 68%, 84%, and 93%, the average frequency shifts of the sensors were recorded as 10.0, 22.7, 36.2, 58.8, and 89.8 kHz, respectively. In addition, when the RH was changed back to 30% after each test, the resonant frequency was quickly recovered to its initial value.

Fig. 8(b) shows the frequency shift as a function of RH for three groups of 7-layer BC SAW sensors, fabricated in the same batch process. The frequency shift increases nonlinearly with the RH with repeatable results observed among different devices. When the RH is higher than 80%, significant changes in frequency shift were obtained. This may be attributed to the fact that

significant water condensation occurs at higher RH values, which leads to significant mass loading effects as widely reported in literature [34].

The detection performance of seven-layer BC SAW humidity sensor was further studied in the low RH range (5% - 25% RH) because of its importance for food and pharmaceutical manufacturing. In this study, the low humidity environment was realized by introducing dry N_2 into the enclosed chamber. As shown in Fig. 8 (c), the frequency shift of the sensor has a good linear relationship with the RH value when the value is below 25%. This further proves that the frequency shift of the sensor at a lower RH value is due to only the mass loading effect caused by water molecules adsorbed on the BC film. Whereas at higher RH levels, the frequency shift is not only due to the mass loading effect, but also due to the additive effect of water condensation.

3.3 Performances of BC SAW humidity sensor

Fast response and recovery are critical in practical humidity sensing applications. The dynamic frequency shifts of the 7-layer BC SAW device obtained during the response and recovery processes are shown in Figs. 9(a) and 9(b), respectively. A gradual increase in the response time was observed with increasing RH levels, because not only water molecules are adsorbed on the surface of the BC film at higher humidity levels, but also significant condensation of water molecules occurs. It is relatively difficult to release the condensed water molecules, thus causing the increased response and recovery times. For the humidity sensor in this work, the durations to reach 90% of the response levels were measured to be 3 s, 5 s, 7 s, 8 s, and 12 s when the RH values were increased from 30% to 43%, 56%, 68%, 84%, and 93%, respectively. When the humidity was returned to 30%, the durations for the frequency signals to return back to 10% of their original values were measured to

be 3 s, 3 s, 4 s, 4 s, 5 s, respectively.

In order to compare with the performance of other sensors reported in the literature, we detected the humidity sensing with RH values increased from 10% to 93% and then restored to 10% afterwards. The response time was found to increase only by one second and the recovery time increased by only two seconds.Table 1 lists the response and recovery times of the BC based SAW sensor with those of the humidity sensors reported in the literature. Among the reported SAW humidity sensors, the recovery time of our sensor is significantly shorter than the others reported in literature. Moreover, compared with the performance of different types of humidity sensors available in the commercial market, the response time and recovery time of our sensors are shorter or comparable as listed in Table 2 [35].

In the environment with an RH value of 30%, temperature sensitivity of the humidity sensor was characterized within a temperature range from 25 to 60^{o}C. Fig. 10 shows a slight decrease in resonant frequency of the sensor with temperature, with a very good linearity. TCF is often used to describe the effect of temperature changes on sensor response, and the TCF is defined as

$$TCF = \frac{\Delta f}{f_0 \bullet \Delta T} \tag{3}$$

where f_0 is 200 MHz in this study, Δf and ΔT are the changes of resonant frequency and temperature. A very small TCF value of -0.12 ppm/^{o}C was extracted for the 7-layer BC SAW humidity sensor based on the results presented in Fig 10, indicating the insensitivity of the sensor to the minor changes in temperature. Compared to the other SAW devices listed in Table 3, the BC humidity sensor has significant advantages in terms of thermal stability.

In order to study, the selectivity, we further tested the frequency shift of the BC SAW humidity sensor at two humidity levels of 43% RH and 93% RH by introducing different gases such as NH_3,

H_2, CO, HCl and C_2H_5OH. Results showed that when these testing gas concentration was 500 ppm, the frequency shift of the BC SAW humidity sensor due to adding the other types of gases are insignificant compared with those due to the humidity changes, as shown in Fig. 11. This indicates that the influences of introduction of other types of gases does not show significant influence on the humidity sensing. However, it should be noted that this SAW humidity sensor has a slightly higher responses to ammonia at a very high humidity level, although at a low humidity level, the ammonia response is not significantly different from other gases. The response to ammonia at a higher humidity level can be attributed to the adsorption of ammonia gas at a high humidity level on the surface of the BC where water molecules are condensed to form a moisture layer. Strong adsorption of NH_3 in moisture or water layer has been widely reported [36].

The repeatability of the Layer-7 BC SAW humidity sensor was further studied by cycling the RH value between 30% to 93% and then repeated for five cycles. The results are shown in Fig. 12(a). The variation in the frequency shift was less than 5% during the measurement cycles, indicating a good short-term repeatability. The sensor was also tested repeatedly for its long-term stability by keeping it in a chamber with 30%, 43%, 56%, 68%, 84%, and 93% RH for one-month intervals. As shown in Fig. 12(b), the BC SAW humidity sensor exhibited a fluctuation value less than 2% at a lower RH of 43%. Even at a high RH of 93%, the fluctuation in resonant frequency was less than 5%. These experiments revealed that the BC SAW humidity sensor has a good long-term stability.

4. Conclusions

We fabricated BC SAW humidity sensors on ST-cut quartz substrates in this study. The three-dimensional network structure of the BC film and large numbers of pores contribute to the

water adsorption within the membrane. The hydrogen bonding of the surface functional group hydroxyl groups with water molecules enables the BC membrane to effectively adsorb water molecules. This study reveals the mass loading effect as the fundamental mechanism for the frequency shift of SAW sensors as compared to the acoustoelectric effects. The frequency shift of the sensor at a low RH value of less than 30% exhibits a better linear relationship with humidity. Whereas the frequency shift of the BC film increases exponentially with increasing humidity when the RH value exceeds 80%. In addition, a thicker BC layer has more hydrophilic hydroxyl groups, providing more adsorption sites for water molecules. However, excessive increase in the layer thickness also causes an increase in insertion loss, thus deteriorating the frequency signal. The SAW humidity sensor coated with a BC layer on a quartz substrate has achieved with fast response and recovery performance, as well as thermal stability, good short-term and long-term repeatability.

Acknowledgments

This study was supported financially by the Fundamental Research Funds for the Central Universities (A03018023801119), Engineering Physics and Science Research Council of UK (EPSRC EP/P018998/1) and UK Fluidic Network-Special Interest Group of Acoustofluidics, and Newton Mobility Grant (IE161019) through Royal Society and NFSC, and Royal Academy of Engineering: Research Exchange between UK and China.

References

[1] I.E. Kuznetsova, V.I. Anisimkin, V.V. Kolesov, V.V. Kashin, V.A. Osipenko, S.P. Gubin, S.V. Tkachev, E. Verona, S. Sun, A.S. Kuznetsova, Sezawa wave acoustic humidity sensor based on graphene oxide sensitive film with enhanced sensitivity, Sens. Actuators B 272 (2018) 236-242.

https://doi.org/10.1016/j.snb.2018.05.158.

[2] C.R. Zamarreño, M. Hernaez, I. Del Villar, I.R. Matias, F.J. Arregui, Tunable humidity sensor based on ITO-coated optical fiber, Sens. Actuators B 146 (2010) 414-417. https://doi.org/10.1016/j.snb.2010.02.029.

[3] D. Lu, Y. Zheng, A. Penirschke, R. Jakoby, Humidity sensors based on photolithographically patterned PVA films deposited on SAW resonators, IEEE Sens. J. 16 (2016) 13-14. https://doi.org/10.1109/JSEN.2015.2468082.

[4] X.L. He, D.J. Li, J. Zhou, W.B. Wang, W.P. Xuan, S.R. Dong, H. Jin, J.K. Luo, High sensitivity humidity sensors using flexible surface acoustic wave devices made on nanocrystalline ZnO/polyimide substrates, J. Mater. Chem. *C* 1 (2013) 6210-6215. https://doi.org/10.1039/C3TC31126K.

[5] Y. Komazaki, S. Uemura, Stretchable, Printable, and Tunable PDMS-CaCl2 Microcomposite for Capacitive Humidity Sensors on Textiles, Sens. Actuators B 297 (2019) 126711. https://doi.org/10.1016/j.snb.2019.126711.

[6] L. Luo, M. Yuan, H. Sun, T. Peng, T. Xie, Q. Chen, J. Chen, Effect of calcination temperature on the humidity sensitivity of TiO_2/graphene oxide nanocomposites, Mater. Sci. Semicond. Process. 89 (2019) 186-193. https://doi.org/10.1016/j.mssp.2018.09.019.

[7] S. Kano, K. Kim, M. Fujii, Fast-response and flexible nanocrystal-based humidity sensor for monitoring human respiration and water evaporation on skin, ACS Sens. 2 (2017) 828-833. https://doi.org/10.1021/acssensors.7b00199.

[8] R. Rimeika, D. Ciplys, V. Poderys, R. Rotomskis, M.S. Shur, Fast-response and low-loss surface acoustic wave humidity sensor based on bovine serum albumin-gold nanoclusters film, Sens. Actuators B 239 (2017) 352-357. https://doi.org/10.1016/j.snb.2016.07.161.

[9] J. Devkota, P.R. Ohodnicki, D.W. Greve, SAW sensors for chemical vapors and gases, Sensors 17 (2017) 801. https://doi.org/10.3390/s17040801.

[10] X.H. Le, X.Y. Wang, J.T. Pang, Y.J. Liu, B. Fang, Z. Xu, C. Gao, Y. Xu, J. Xie, A high performance humidity sensor based on surface acoustic wave and graphene oxide on AlN/Si layered structure, Sens. Actuators B 255 (2018) 2454-2461. https://doi.org/10.1016/j.snb.2017.09.038.

[11] Y. Liu, H. Huang, L.L. Wang, D.P. Cai, B. Liu, D.D. Wang, Q.H. Li, T.H. Wang, Electrospun CeO_2 nanoparticles/PVP nanofibers based high-frequency surface acoustic wave humidity sensor,

Sens. Actuators B 223 (2016) 730-737. https://doi.org/10.1016/j.snb.2015.09.148.

[12] Y.L. Tang, Z.J. Li, J.Y. Ma, L. Wang, J. Yang, B. Du, Q.K. Yu, X.T. Zu, Highly sensitive surface acoustic wave (SAW) humidity sensors based on sol-gel SiO_2 films: Investigations on the sensing property and mechanism, Sens. Actuators B 215 (2015) 283-291. https://doi.org/10.1016/j.snb.2015.03.069.

[13] X.T. Ma, Y. Lou, X.B. Chen, Z. Shi, Y. Xu, Multifunctional flexible composite aerogels constructed through in-situ growth of metal-organic framework nanoparticles on bacterial cellulose, Chem. Eng. J. 356 (2019) 227-235. https://doi.org/10.1016/j.cej.2018.09.034.

[14] S. Sheykhnazari, T. Tabarsa, M. Mashkour, A. Khazaeian, A. Ghanbari, Multilayer bacterial cellulose/resole nanocomposites: Relationship between structural and electro-thermo-mechanical properties, In. J. Biol. Macromol. 120 (2018) 2115-2122. https://doi.org/10.1016/j.ijbiomac.2018.09.047.

[15] A. Dobashi, J. Maruyama, Y.H. Shen, M. Nandi, H. Uyama, Activated carbon monoliths derived from bacterial cellulose/polyacrylonitrile composite as new generation electrode materials in EDLC, Carbohydr. Polym. 200 (2018) 381-390. https://doi.org/10.1016/j.carbpol.2018.08.016.

[16] R.S. Tabatabaee, H. Golmohammadi, S.H. Ahmadi, Easy diagnosis of jaundice: A smartphone-based nanosensor bioplatform using photoluminescent bacterial nanopaper for point-of-care diagnosis of hyperbilirubinemia, ACS Sens. 4 (2019) 1063-1071. https://doi.org/10.1021/acssensors.9b00275.

[17] N. Tonouchi, T. Tsuchida, F. Yoshinaga, T. Beppu, S. Horinouchi, Characterization of the biosynthetic pathway of cellulose from glucose and fructose in acetobacter xylinum, Biosci. Biotechnol. Biochem. 60 (1996) 1377-1379. https://doi.org/10.1271/bbb.60.1377.

[18] K. Zaar, Visualization of pores (export sites) correlated with cellulose production in the envelope of the gram-negative bacterium acetobacter xylinum, J. Cell Biol. 80 (1979) 773-777. https://doi.org/10.1083/jcb.80.3.773.

[19] R. Jonas, L.F. Farah, Production and application of microbial cellulose, Polym. Degrad. Stabil. 59 (1998) 101-106. https://doi.org/10.1016/S0141-3910(97)00197-3.

[20] T. Naritomi, T. Kouda, H. Yano, F. Yoshinaga, Effect of lactate on bacterial cellulose production from fructose in continuous culture, J. Ferment. Bioeng. 85 (1998) 89-95. https://doi.org/10.1016/S0922-338X(97)80360-1.

[21] D. Klemm, D. Schumann, U. Udhardt, S. Marsch, Bacterial synthesized cellulose-artificial blood vessels for microsurgery, Prog. Polym. Sci. 26 (2001) 1561-1603. https://doi.org/10.1016/S0079-6700(01)00021-1.

[22] A. Svensson, E. Nicklasson, T. Harrah, B. Panilaitis, D.L. Kaplan, M. Brittberg, P. Gatenholm, Bacterial cellulose as a potential scaffold for tissue engineering of cartilage, Biomaterials 26 (2005) 419-431. https://doi.org/10.1016/j.biomaterials.2004.02.049.

[23] W. Hu, S. Chen, B. Zhou, L. Liu, B. Ding, H. Wang, Highly stable and sensitive humidity sensors based on quartz crystal microbalance coated with bacterial cellulose membrane, Sens. Actuators B 159 (2011) 301-306. https://doi.org/10.1016/j.snb.2011.07.014.

[24] Y.Q. Fu, J.K. Luo, N.T. Nguyen, A.J. Walton, A.J. Flewitt, X.T Zu, Y. Li, G. McHale, A. Matthews. E. Iborra H. Du, W.I. Milne, Advances in piezoelectric thin films for acoustic biosensors, acoustofluidics and lab-on-chip applications, Progress in Mater Sci. 89 (2017) 31-91. https://doi.org/10.1016/j.pmatsci.2017.04.006.

[25] B. Liu, X. Chen, H. Cai, M. Mohammad, X. Tian, L. Tao, Y. Yang, T. Ren, Surface acoustic wave devices for sensor applications, J. Semicond 2 (2016) 1-9. https://doi.org/10.1088/1674-4926/37/2/021001.

[26] A. Afzal, N. Iqbal, A. Mujahid, R. Schirhagl. Advanced vapor recognition materials for selective and fast responsive surface acoustic wave sensors: A review, Anal. Chim. Acta 787 (2013) 36-49. https://doi.org/10.1016/j.aca.2013.05.005.

[27] L. Greenspan, Humidity fixed points of binary saturated aqueous solutions, J. Res. Natl. Bur. Stand. 81 (1977) 89–96. https://pdfs.semanticscholar.org/9a90/c8e8fb71c152ae3bacf9904e6c761cdf9de7.pdf.

[28] C. Eaborn, The sadtler handbook of infrared spectra: edited by W.W. Simons, Heyden and Son, Ltd, London, J. Organomet. Chem. 171 (1979) 44. https://doi.org/10.1016/S0022-328X(00)81552-1.

[29] S. Okuda, T. Ono, Y. Kanai, T. Ikuta, M. Shimatani, S. Ogawa, K. Maehashi, K. Inoue, K. Matsumoto, Graphene surface acoustic wave sensor for simultaneous detection of charge and mass, ACS Sens. 3 (2018) 200-204. https://doi.org/10.1021/acssensors.7b00851.

[30] A. Müller, G. Konstantinidis, V. Buiculescu, A.Dinescu, A. Stavrinidis, A. Stefanescu, G. Stavrinidis, I. Giangu, A. Cismaru, A. Modoveanu, GaN/Si based single SAW resonator temperature sensor operating in the GHz frequency range, Sens. Actuators A 209 (2014) 115-123.

https://doi.org/10.1016/j.sna.2014.01.028.

[31] V.B. Raj, A.T. Nimal, Y. Parmar, M.U. Sharma, V. Gupta, Investigations on the origin of mass and elastic loading in the time varying distinct response of ZnO SAW ammonia sensor, Sens. Actuators B 166 (2012) 576-585. https://doi.org/10.1016/j.snb.2012.03.013.

[32] W.P. Jakubik, Surface acoustic wave-based gas sensors, Thin Solid Films 520 (2011) 986-993. https://doi.org/10.1016/j.tsf.2011.04.174.

[33] J.D.N. Cheeke, Z. Wang, Acoustic wave gas sensors, Sens. Actuators B 59 (1999) 146-153. https://doi.org/10.1016/s0925-4005(99)00212-9.

[34] J. Weremczuk, R. Iwaszko, R. Jachowicz, The method of water molecules counting during condensation process in the dew point detector, Sens. Actuators B 175 (2012) 137-141. https://doi.org/10.1016/j.snb.2012.01.014.

[35] S.A. Kolpakov, N.T. Gordon, C. Mou, K. Zhou, Toward a new generation of photonic humidity sensors, Sensors 14 (2014) 3986-4013. https://doi.org/10.3390/s140303986.

[36] Y. Liu, H. Huang, L.L. Wang, D.P. Cai, B. Liu, D.D. Wang, Q.H. Li, T.H. Wang, Electrospun CeO_2 nanoparticles/PVP nanofibers based high-frequency surface acoustic wave humidity sensor, Sens. Actuators B 223 (2016) 730-737. https://doi.org/10.1016/j.snb.2015.09.148.

[37] X. Le, Y. Liu, L. Peng, J. Pang, Z. Xu, C. Gao, J. Xie, Surface acoustic wave humidity sensors based on uniform and thickness controllable graphene oxide thin films formed by surface tension, Microsyst. Nanoeng. 5 (2019) 1-10. https://doi.org/10.1038/s41378-019-0075-0.

[38] W. Xuan, M. He, N. Meng, X. He, W. Wang, J. Chen, T. Shi, T. Hasan, Z. Xu, Y. Xu, J.K. Luo, Fast response and high sensitivity ZnO/glass surface acoustic wave humidity sensors using graphene oxide sensing layer, Sci. Rep. 4 (2014) 1-9. https://doi.org/10.1038/srep07206.

[39] S. Lei, C. Deng, Y. Chen, Y. Li, A novel serial high frequency surface acoustic wave humidity sensor, Sens. Actuators A 167 (2011) 231-236. https://doi.org/10.1016/j.sna.2011.01.020.

[40] X.Y. Du, M.E. Swanwick, Y.Q. Fu, J.K. Luo, A.J. Flewitt, D.S. Lee, S. Maeng, W.I. Milne, Surface acoustic wave induced streaming and pumping in 128^{o} Y-cut $LiNbO_3$ for microfluidic applications, J. Micromech Microeng 19 (2009) 035016. https://doi.org/10.1088/0960-1317/19/3/035016.

[41] S.V. Biryukov, H. Schmidt, M. Weihnacht, Gyroscopic effect for SAW in common piezoelectric crystals, 2009 IEEE International Ultrasonics Symposium, 20-23 (2009) 2133–2136.

https://doi.org/10.1109/ULTSYM.2009.5441457.

[42] I. Ben Salah, M.H. Ben Ghozlen, Rayleigh waves in piezoelectric material, Phys. Procedia 2 (2009) 1377–1383. https://doi.org/10.1016/j.phpro.2009.11.105.

Biographies

Jing-Long Wang graduated from the College of Electrical Information Engineering of Anhui University of Science and Technology in 2017 with a bachelor's degree. He is a graduate student in School of Physical at University of Electronic Science and Technology of China. His current interests include sensor research on nanomaterials and functional films and surface acoustic wave devices.

Yuan-Jun Guo received his Ph.D. from Shanghai Institute of Optics and Fine Mechanics, Chinese Academy of Sciences in 2006. From December 2016, he became a Professor in School of Physical, University of Electronic Science and Technology of China. His current research interests focus on sensing devices using acoustic wave technology, microfluidics and interaction between laser and solid material.

Deng-Ji Li obtained his B.S. degree in School of Physic, Wuhan University. He is a postgraduate student in Institute of Fundamental and Frontier Sciences at University of Electronic Science and Technology of China. His current research interests focus on sensing devices using acoustic wave technology applications of nanomaterials and novel functional materials.

Gong-Di Long obtained his B.S. degree in School of photoelectric technology, Chengdu University of Information Technology in 2016. He is a Master Degree Candidate in School of Physical at University of Electronic Science and Technology of China. His current research interests focus on sensing devices using acoustic wave technology, preparation and research of magnetic materials.

Qing-Bo Tang obtained his B.S. degree in School of Computer and Information, China Three Gorges University in 2016. He is a Master Degree Candidate in School of Physical at University of Electronic Science and Technology of China. His current research interests focus on sensing devices using acoustic wave technology, microfluidics and interaction between laser and solid material.

Xiao-Tao Zu received his Ph.D. degree from Sichuan University in 2002. He is a Professor in Institute of Fundamental and Frontier Sciences at University of Electronic Science and Technology of China. His research interests include photoelectric materials, smart materials, composite nanomaterials and their industrial applications.

Jin-Yi Ma received his Ph.D. degree from Tianjin University in 2003. He is a senior research fellow in Sichuan Institute of Piezoelectric and Acousto-optic Technology. His research area is on piezoelectric materials and industrial applications of the acoustic-optical device.

Bo Du received his M.S. degree from University of Electronic Science and Technology of China in 2010. He is a senior engineer in Sichuan Institute of Piezoelectric and Acousto-optic Technology. His research area is on piezoelectric materials and piezoelectric sensors.

Yong-Liang Tang obtained his PH.D. degree from University of Electronic Science and Technology

of China in 2017. He is now an associate Professor in School of Physical Science and Technology at Southwest Jiaotong University. His present interests include applications of nanomaterials and functional thin films for sensors and surface acoustic wave (SAW) devices.

Hamdi Torun (HT), joined the UNN in 2017 as a Vice-Chancellor Senior Fellow. Previously, he was an associate professor at Bogazici University, Turkey. He is a co-founder of GlakoLens, a biomedical spinoff company. He received Technology Award from Elginkan Foundation, Turkey in 2016, Young Scientist Award from The Science Academy, Turkey in 2016, Innovator Under 35 Award from MIT Tech Review in 2014, and Marie Curie Fellowship (MC-IRG Grant) in 2011. His expertise is in development of integrated microsystems especially for sensing applications. His research experience includes metamaterial-based biosensors for molecular detection, for glucose detection, and for wireless strain sensing, theoretical understanding of metamaterial structures, novel terahertz devices.

Richard (YongQing) Fu is a professor in the Faculty of Engineering and Environment, University of Northumbria at Newcastle, UK. He obtained his PhD degree from Nanyang Technological University, Singapore, and then worked as a Research Fellow in Singapore-Massachusetts Institute of Technology Alliance, and a Research Associate in University of Cambridge. He was a lecturer in Heriot-Watt University, Edinburgh, UK, and then a Reader in Thin Film Centre in University of West of Scotland, Glasgow, UK, before moving to Newcastle, UK. He has extensive experience in smart thin film/materials, biomedical microdevices, energy materials, lab-on-chip, micromechanics, MEMS, nanotechnology, sensors and microfluidics. He published over 360 science citation index (SCI) journal papers and his current SCI H-index is 45 with over 8500 citations. He is associate editor/editorial board members for seven international journals including *Scientific Report, Nanosci. Nanotech. Lett.*

Table 1. Comparisons of response time and recovery time of different humidity sensors.

Sensor	Structure	Sensing material	RH range	t_{res}/t_{rec} (s)	Reference
Capacitive	Textile substrate	polydimethylsiloxane and $CaCl_2$	30%-60%	120/-	[5]
Resistance	Ag-Pd electrode	TiO_2/graphene oxide nanocomposites	11%-93%	129/59	[6]
SAW	AlN	Graphene oxide (210 nm)	15%-80%	10/9	[37]
QCM	Quartz crystal microbalance	Bacterial cellulose	60%-97%	102/57	[23]
SAW	ST-cut quartz	Bacterial cellulose	10%-93%	13/7	This work

Table 2. Performance comparisons of the newly developed SAW sensor with typical commercial humidity sensors.

Sensors	Principle	Response time (s)	Recovery time (s)
SHT15 Polymer	Capacitive	8	8
DHT11	Resistance	10	10
HMT330	Electronic	20	50
This work	SAW	12	5

*The mainstream humidity sensor data on the market shown above were obtained from reference [35].

Table 3. Comparison of TCF values for SAW devices with different substrate material.

Substrate material	TCF(ppm/°C)	Reference
128° Y-cut $LiNbO_3$	-75	[40]
AIN/Si	-22.1	[10]
X-112Y $LiTaO_3$	-18	[41]
ZnO	-15	[42]
42°75’ ST-cut	-0.12	This work

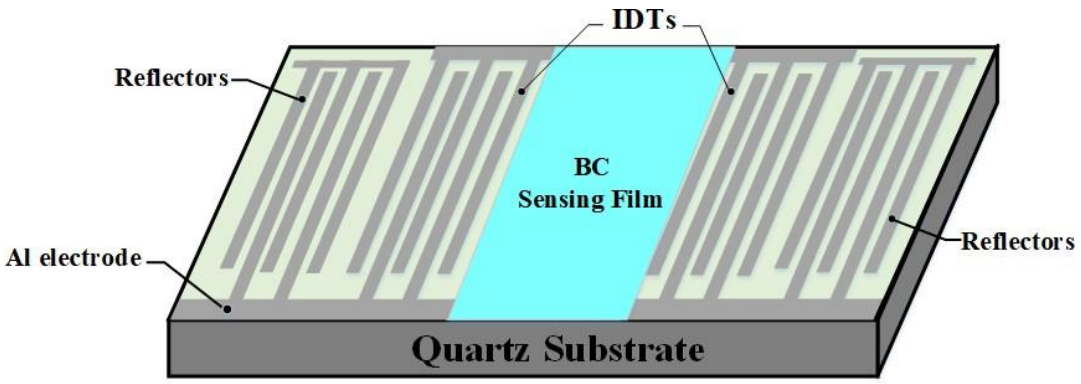

(a)

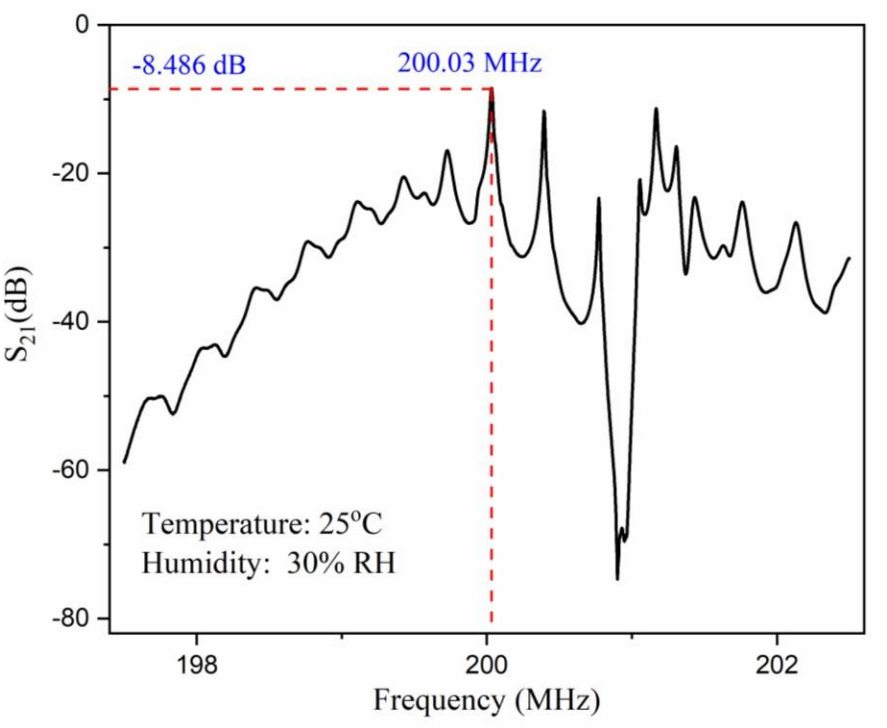

(b)

Fig.1. (a) Schematic illustration of SAW sensor based on an ST-cut quartz substrate; (b) S-parameter detection diagram of SAW resonator.

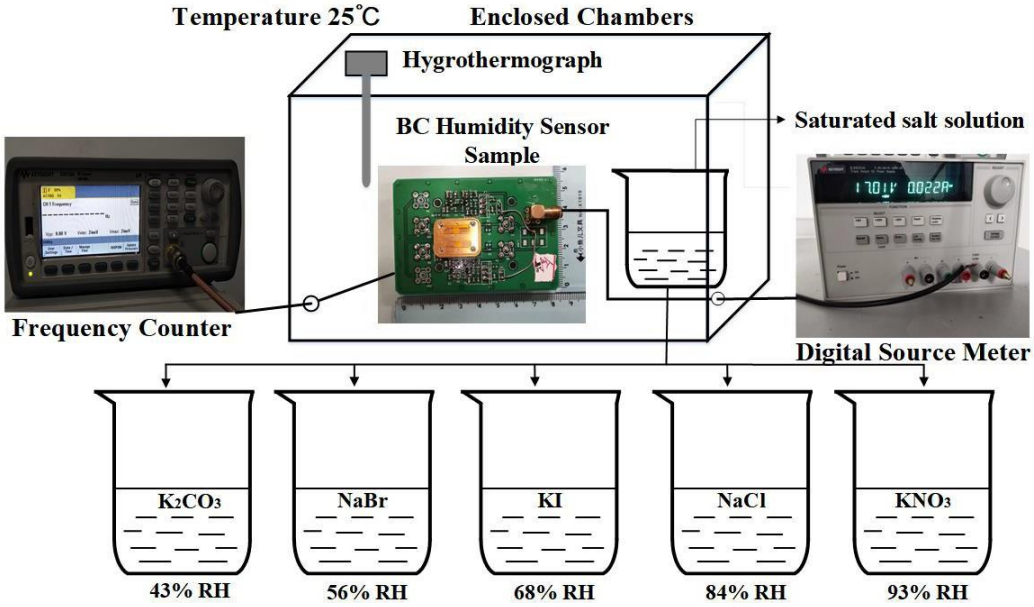

Fig.2. Experimental set-up for SAW humidity sensing and illustration of humidity control method using the saturated salt solution.

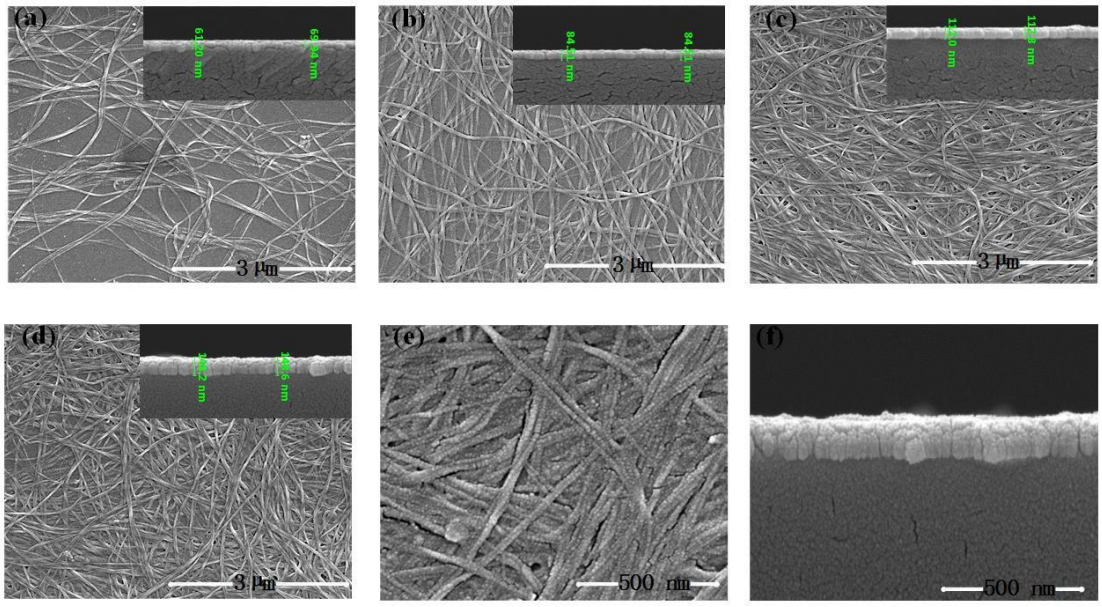

Fig.3. SEM images of surface and cross-section morphologies of the BC films coated with different layers, (a) 1 layer; (b) 3 layers; (c) 5 layers; (d) 7 layers (scale bars on the large image are 3 μm, the scale bars of the upper right image is 1 μm), (e) and (f) are enlarged surface and cross-section views of the 7 layer film (scale bars are 500 nm).

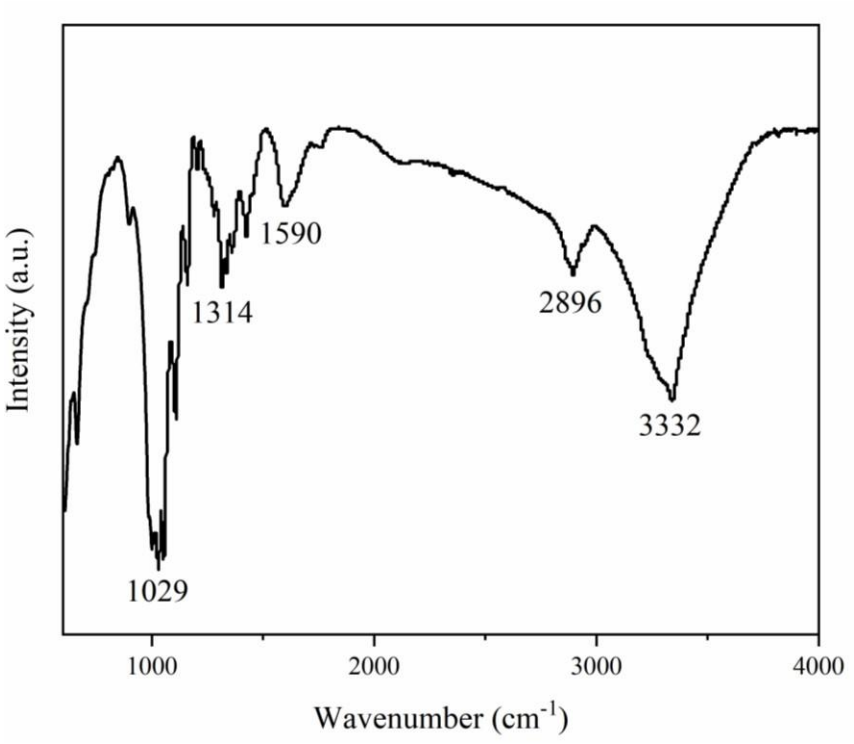

(a)

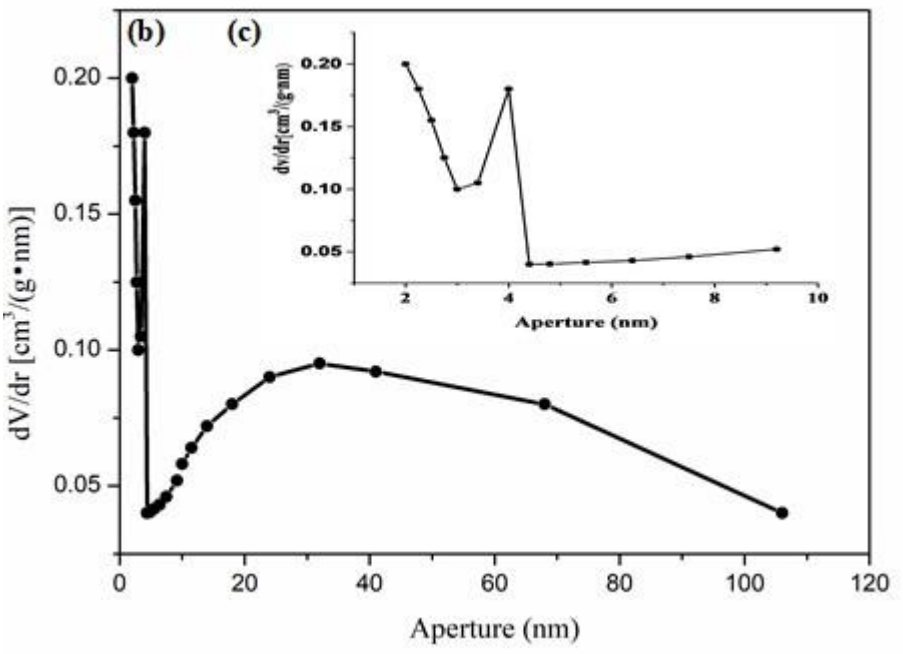

(b)

Fig.4. (a) FTIR spectra of BC materials showing that the surface group has only hydroxyl groups; (b) pore size distribution map of BC material; (c) a partial enlarged view of (b).

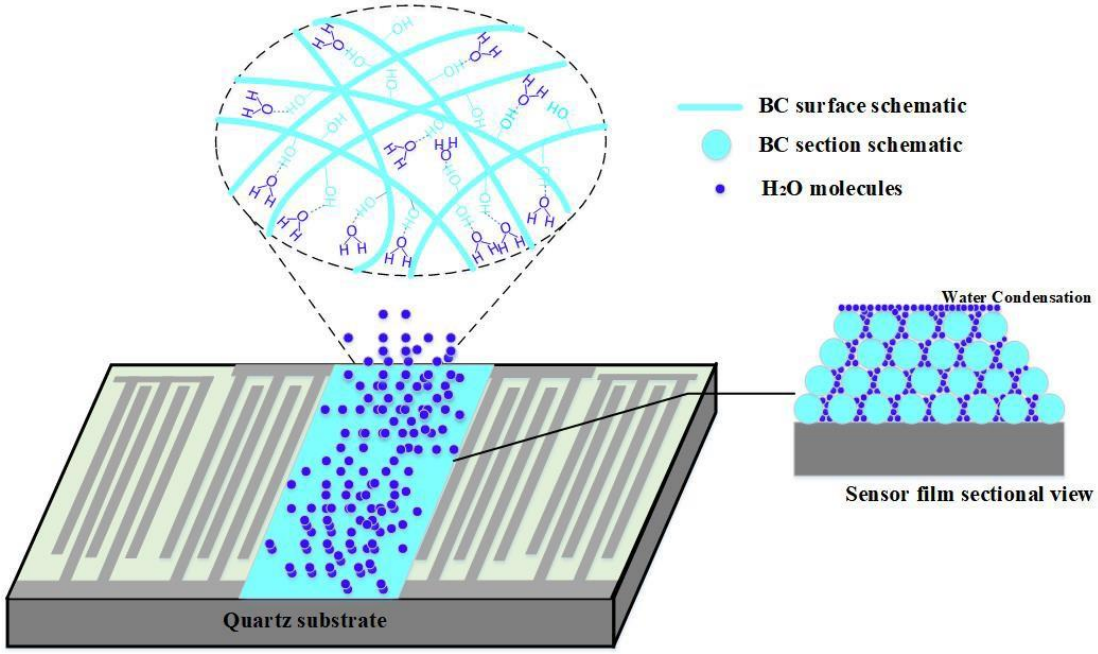

Fig. 5. Schematic illustrations of adsorption of water molecules on the BC layer of the SAW device.

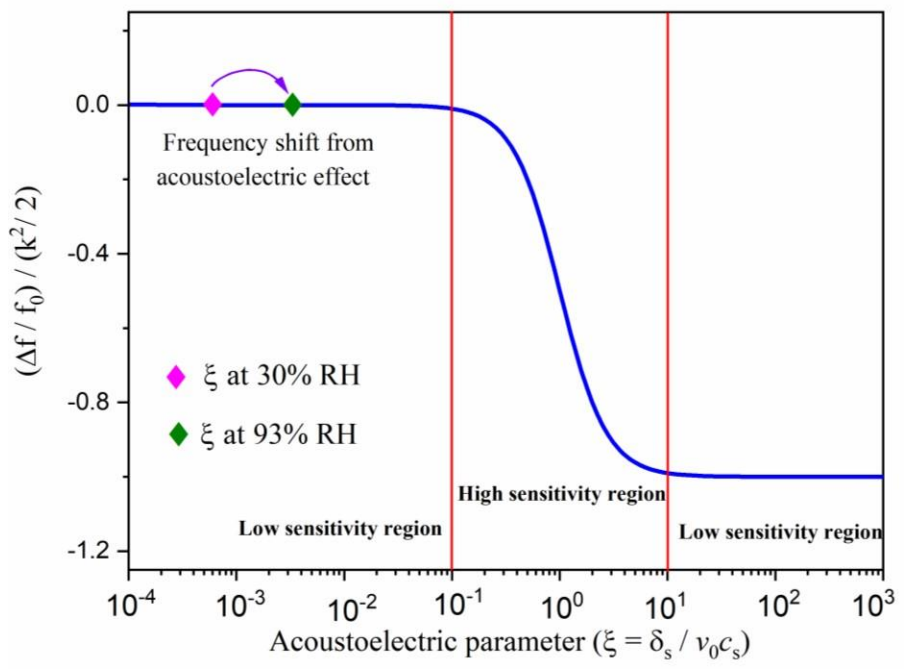

(a)

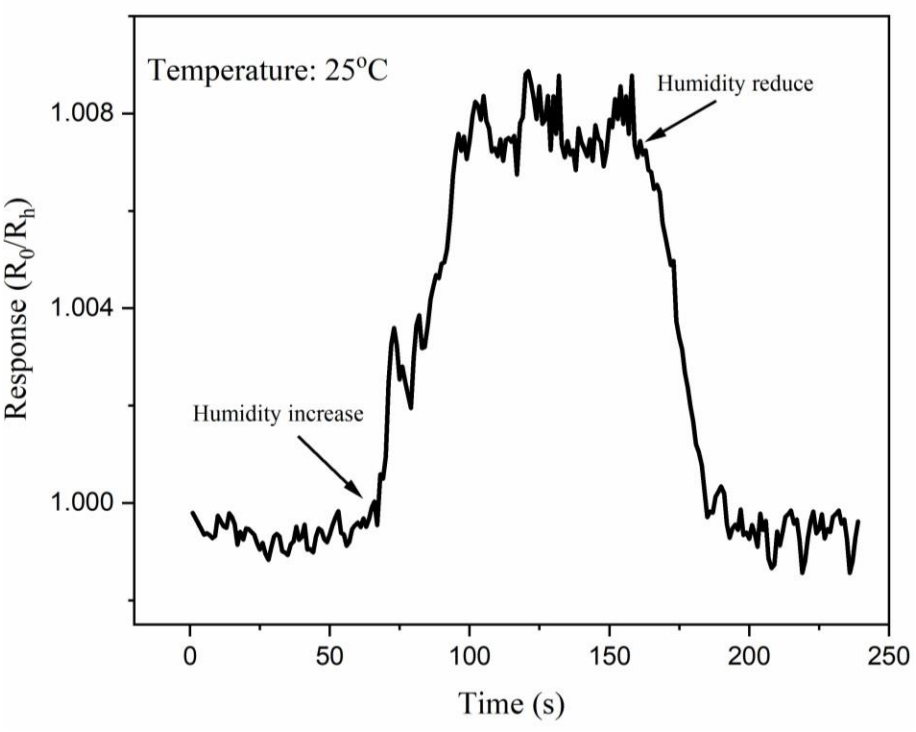

(b)

Fig. 6. (a) Plot of frequency changes of SAW sensor versus acoustoelectric parameter $\xi=\sigma_s/(v_0C_s)$; (b) Resistance responses of BC sensing film ($R=R_h/R_0$) when humidity is changed between 30% and 93% RH.

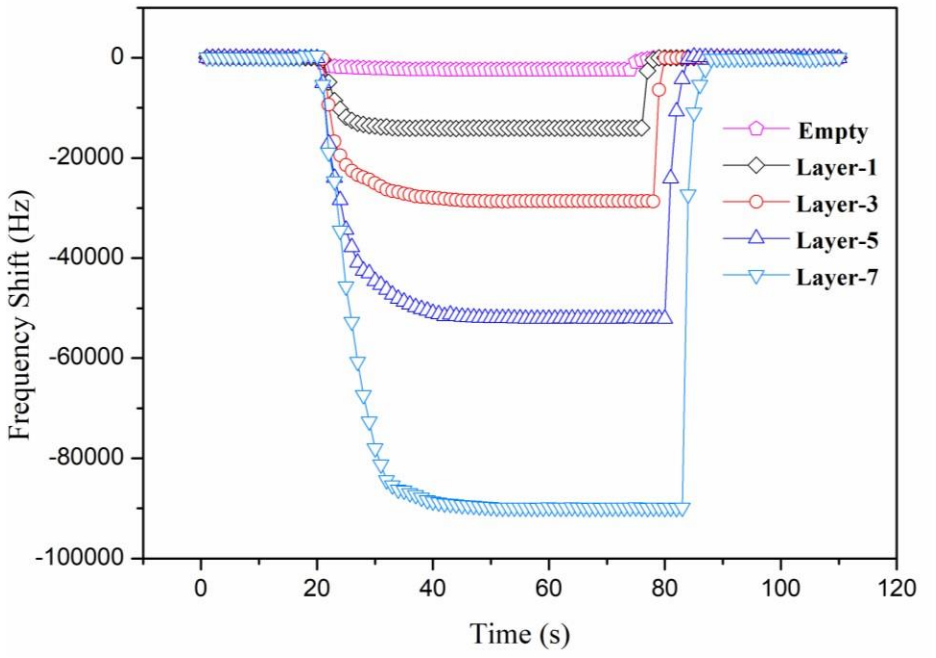

(a)

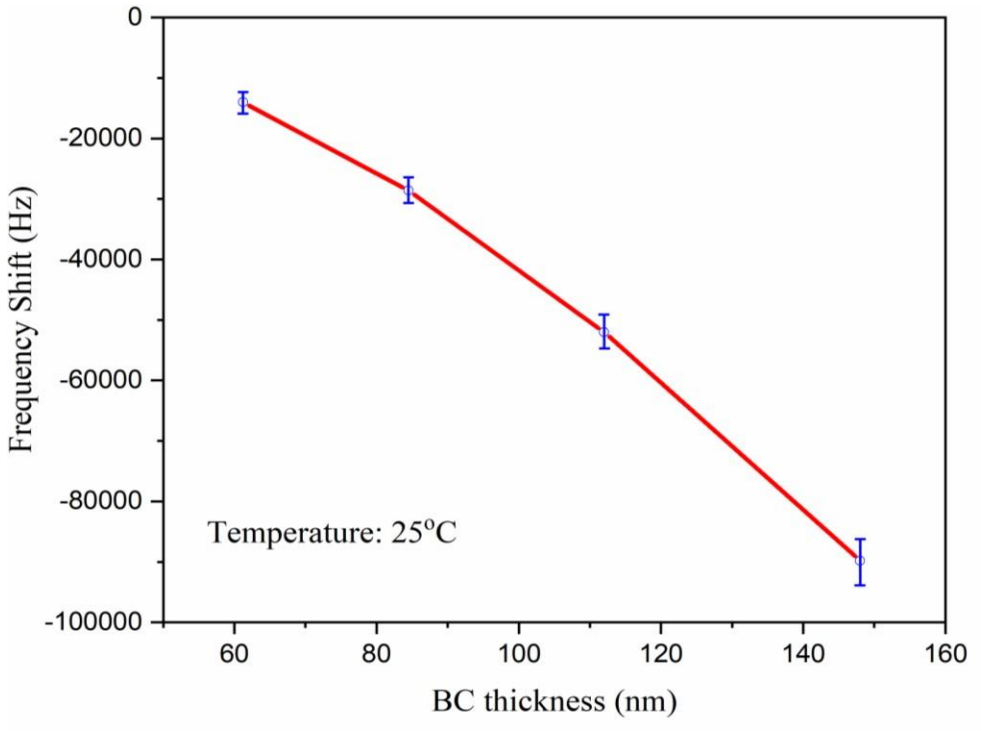

(b)

Fig.7. (a) Frequency shift of SAW device with the BC layers with different thicknesses when relative humidity is increased from 30% to 93%; (b) frequency shift of the SAWdevice as a function of the thickness of BC.

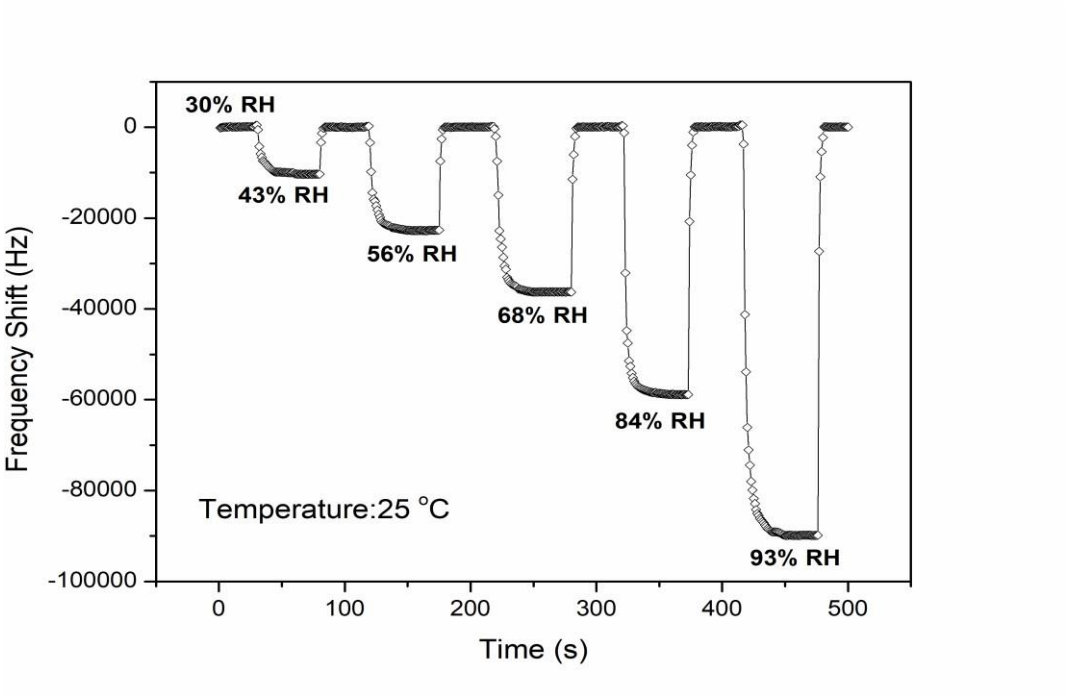
30% RH
43% RH
56% RH
68% RH
84% RH
93% RH
Temperature:25 °C
Frequency Shift (Hz)
Time (s)
0
-20000
-40000
-60000
-80000
-100000
0
100
200
300
400
500

(a)

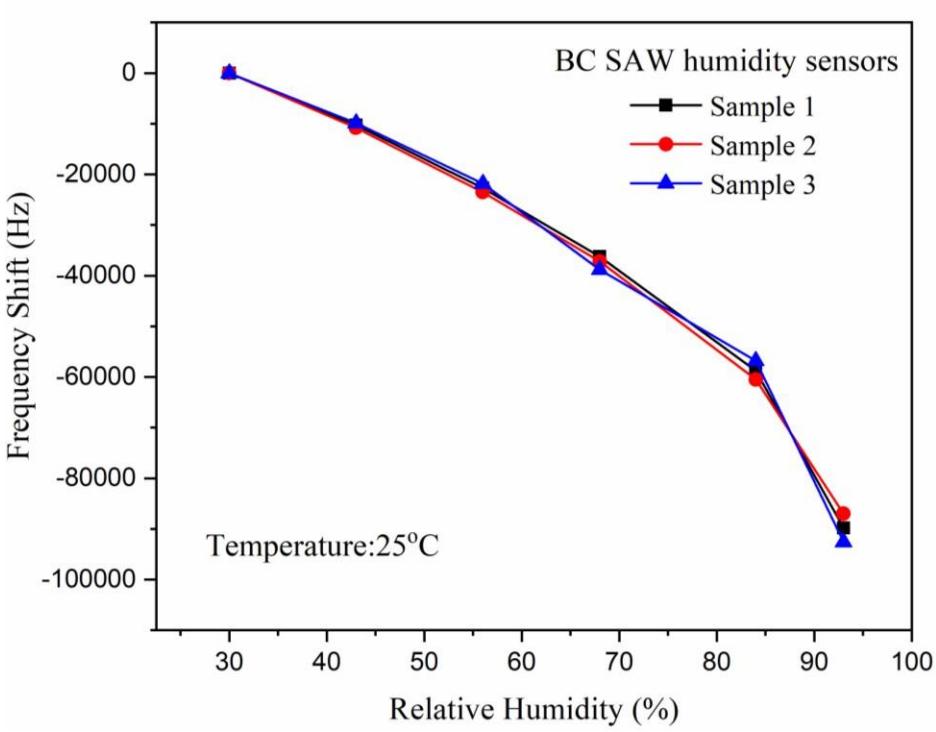
BC SAW humidity sensors
Sample 1
Sample 2
Sample 3
Temperature:25°C
Frequency Shift (Hz)
Relative Humidity (%)
0
-20000
-40000
-60000
-80000
-100000
30
40
50
60
70
80
90
100

(b)

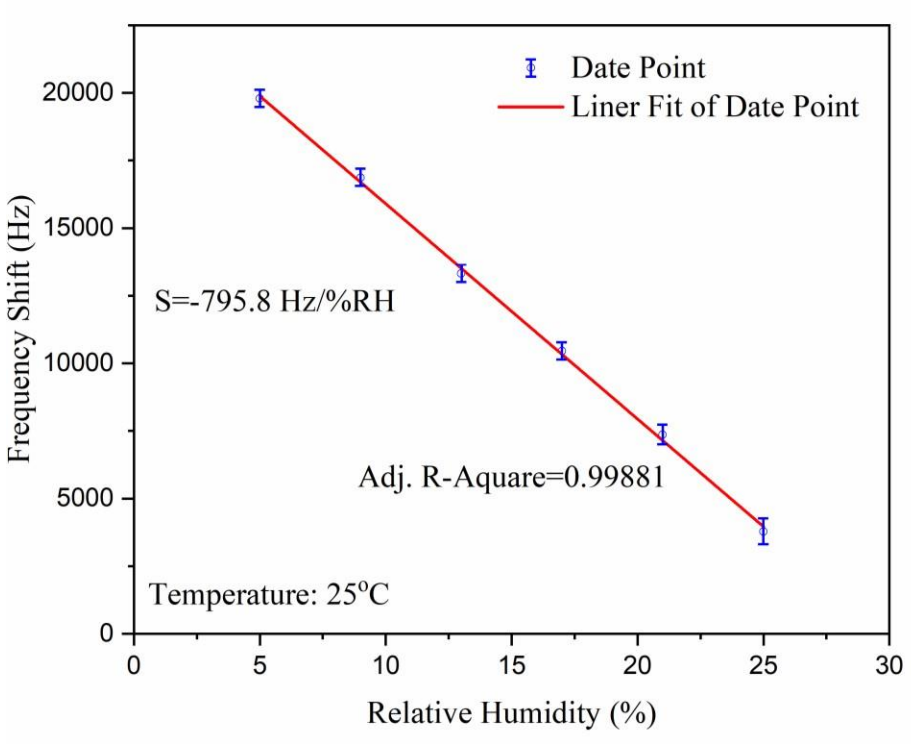

(c)

Fig. 8. (a) Dynamic response of the 7-Layer BC SAW sensor at different relative humidity values; (b) frequency shift of three sensors with the same configurations as a function of RH value; (c) sensing performance of the SAW sensor in low humidity range (5%-25%RH).

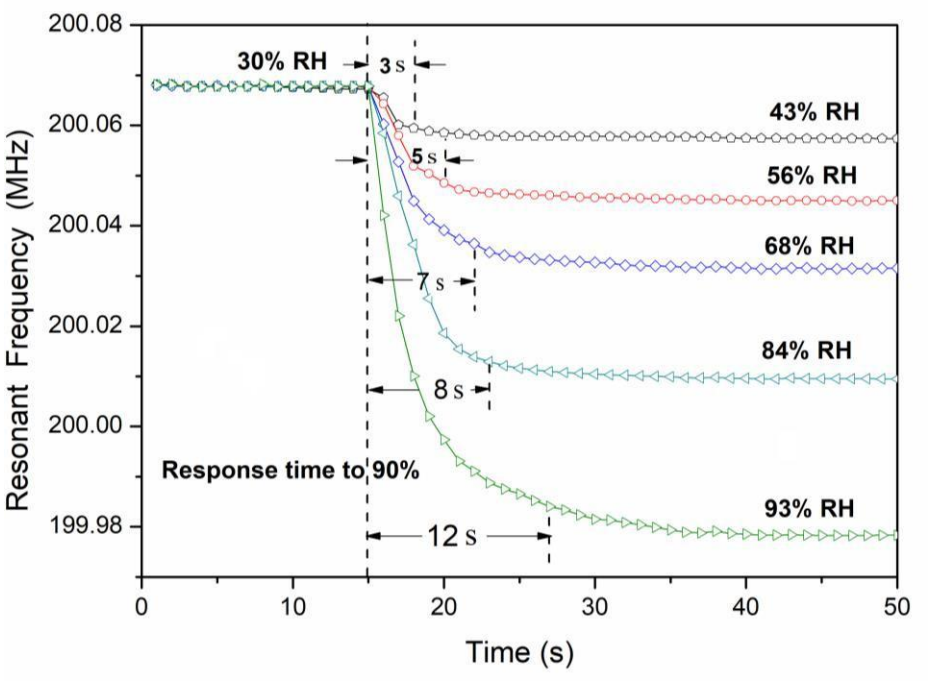

(a)

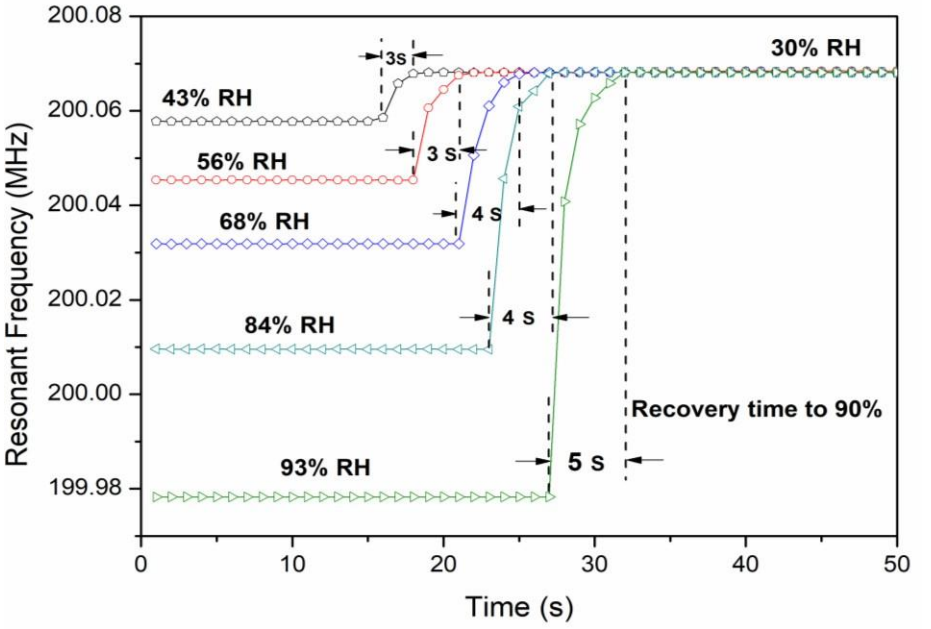

(b)

Fig. 9. (a) Freqeuncy shifts vs Time taken by the Layer-7 BC humidity SAW sensor when the RH value is increased from 30% to 43%, 56%, 68%, 84%, and 93% to reach 90% response; (b) Changes of the resonant signals as a function of time when the RH values was changed from the specific value to 30%.

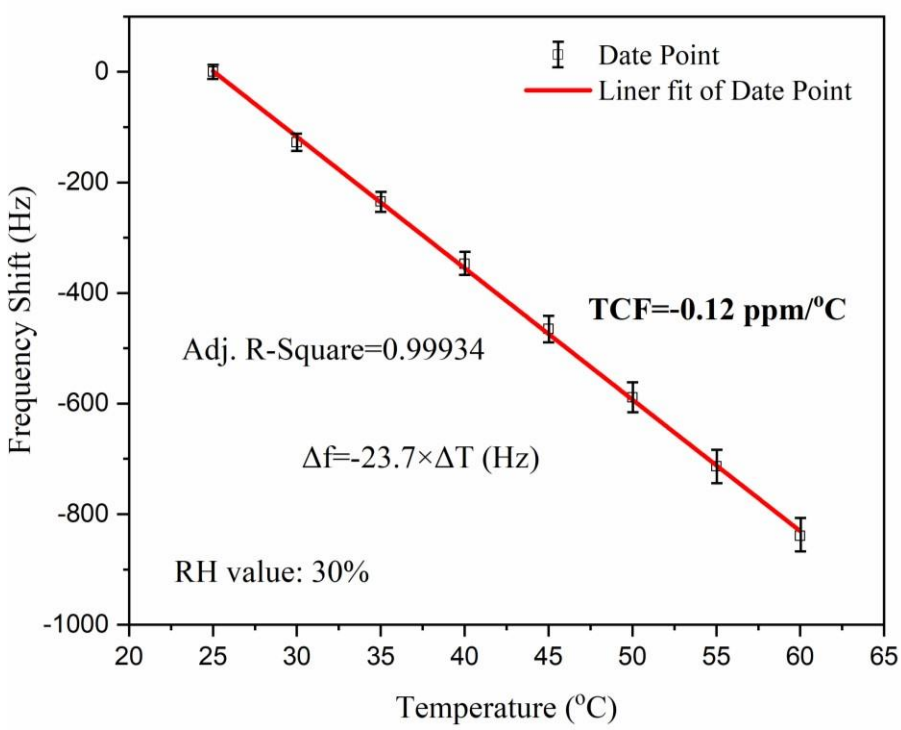

Fig. 10. Variations of the resonant frequencies of the Layer-7 BC humidity sensor versus environment temperatures.

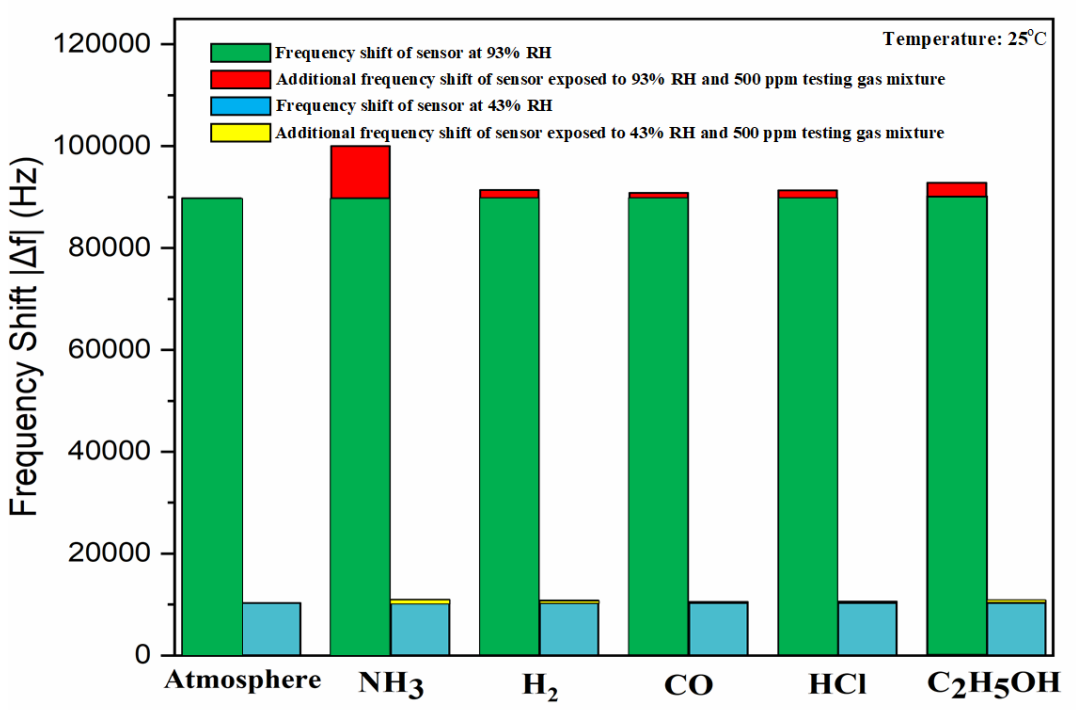

Fig. 11. Effect of different types of gases on sensor humidity detection under conditions of 43% RH and high humidity 93% RH.

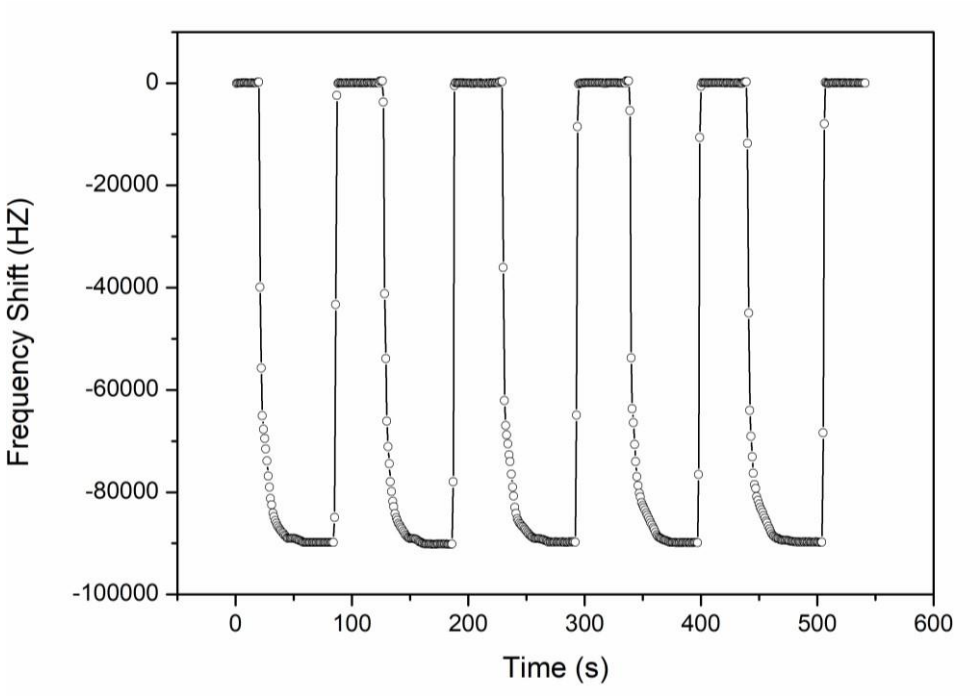

(a)

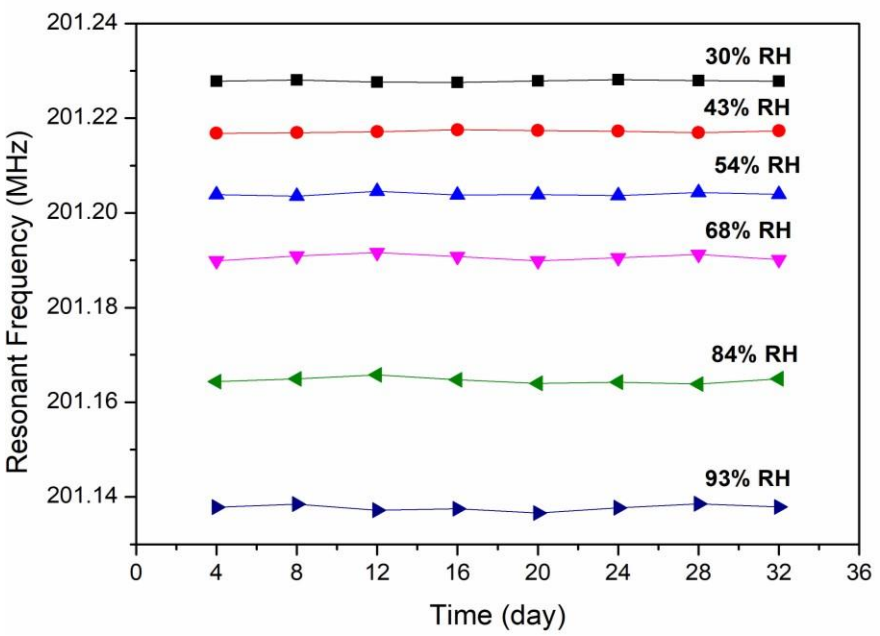

(b)

Fig. 12. (a) Frequency shifts of SAW humidity sensors based on Layer-7 BC film for five humidity cycling tests with the RH values changed between 30% to 93%; (b) the resonant frequency of the SAW humidity sensors tested within one month at different RH values.